Cardiovascular Toxicology (2019) 19:56–61
https://doi.org/10.1007/s12012-018-9473-z

Predictive Role of the Cervical Sympathetic Trunk Ischemia on Lower Heart Rates in an Experimentally Induced Stenoocclusive Carotid Artery Model by Bilateral Common Carotid Artery Ligation

Yavuzer Koza[1] · Ednan Bayram[1] · Mehmet Dumlu Aydin[2] · Canan Atalay[3] · Mehmet Resit Onen[4] · Cengiz Ozturk[5] · Sare Sipal[6] · Elif Demirci[6] · Akin Levent[7]

Published online: 10 July 2018

Abstract

Bilateral common carotid artery ligation (BCCAL) leads to acute craniocervicocerebral ischemia, retrograde blood flow, increased blood pressure, and significant hemodynamic and histomorphological changes at the posterior cerebral vasculature. We examined the potential relationship between denervation injury following BCCAL-induced cervical sympathetic trunk (CST) ischemia and heart rate after permanent BCCAL. Rabbits ($n=25$) were randomly divided into three groups: an unoperated control group (GI, $n=6$); a sham-operated control group (GII, $n=6$), and an experimental group subjected to BCCAL (GIII, $n=13$); and then followed for one month. All animals were then sacrificed and the stellate ganglia (STGs) were examined histologically using stereological methods. The densities of degenerated neurons in the STGs were compared with heart rates and the results were analyzed with the Mann–Whitney U test. The mean normal neuron density in STGs was $10.340 \pm 954/mm^3$ and the degenerated neuron density was $12 \pm 3/mm^3$ in the GI group ($p > 0.5$). The mean heart rates and degenerated neuron densities of STGs were recorded as 267 ± 19/min and $237 \pm 45/mm^3$ in GII ($p < 0.005$ for GII vs. GI); and 190 ± 11/min $1421 \pm 230/mm^3$ in GIII ($p < 0.0001$ for GIII vs. GI and $p < 0.005$ for GIII vs. GII). An inverse and meaningful association was observed between the heart rate and degenerated neuronal density in the STGs. BCCAL may lead to hazardous histomorphological changes in the CST. A high density of degenerated neurons in the STG may provoke excessive sympathetic hypoactivity-related cardiac damage and bradyarrhythmias after stenoocclusive carotid artery diseases.

Keywords Cervical sympathetic trunk ischemia · Common carotid artery · Heart rate

Handling Editor: Y. James Kang.

✉ Yavuzer Koza
yavuzerkoza@hotmail.com

1 Department of Cardiology, Medical Faculty, Ataturk University, Yakutiye, 25100 Erzurum, Turkey

2 Department of Neurosurgery, Medical Faculty, Ataturk University, Erzurum, Turkey

3 Department of Anesthesiology, Medical Faculty, Ataturk University, Erzurum, Turkey

4 Neurosurgery Clinic, Umraniye Education and Research Hospital, Istanbul, Turkey

5 Family Medicine, Osman Gazi Family Health Medicine Center, Erzurum, Turkey

6 Department of Pathology, Medical Faculty, Ataturk University, Erzurum, Turkey

7 Department of Radiology, Medical Faculty, Ataturk University, Erzurum, Turkey

Introduction

Bilateral common carotid artery ligation (BCCAL) causes retrograde blood flow, increased blood pressure, significant hemodynamic and histomorphological changes at the carotico-vertebrobasilar vasculatures, and ischemic degenerative changes in target tissues [1]. BCCAL can lead to cervical sympathetic trunk (CST) ischemia, which leads to degeneration of the CST. This, in turn, inhibits the sympathetic system, which decreases the heart rate and causes rhythm abnormalities. The high neuron density of the stellate ganglion (STG) may accentuate the effect of the sympathetic system on cardiorespiratory organs [2]. Furthermore, STG ischemia may cause sympathetic hypoactivity in the cerebral vasculature and the CST [3].

Previous studies have shown that the ventricular arrhythmias after acute myocardial infarction are associated with

cardiac sympathetic hyperactivity, especially in the left STG [4].

Bilateral STG blockage reduces susceptibility to ischemia-induced sustained ventricular tachycardia. Conscious rats show a reduced susceptibility to ischemia-induced sustained ventricular tachycardia following targeted ablation of cardiac sympathetic neurons [5]. Direct/indirect vagal overactivity triggered by BCCAL and STG ischemia may be dangerous for heart autonomy due to bradycardia [2].

The aim of this study was to examine the possible relationship between the BCCAL-induced CST ischemia and bradyarrhythmias following permanent BCCAL.

Materials and Methods

Experiments were performed on 25 normotensive adult male albino New Zealand rabbits weighing 3.0–4.5 kg. All animal protocols were approved by the Ethics Committee of the Medical Faculty of Atatürk University, and animal care and experiments were performed according to the committee's guidelines. All the animal experiments complied with the Animal Research: Reporting of In Vivo Experiments (ARRIVE) guidelines, and they were conducted in accordance with the National Institutes of Health Guide for the Care and Use of Laboratory Animals (NIH Publications No. 8023, revised 1978). Rabbits were randomly divided into three groups: an unoperated control group (GI, $n=6$); a sham-operated control group without ligation (GII, $n=6$), and an experimental group subjected to BCCAL (GIII, $n=13$). After inducing anesthesia with isoflurane administered through a face mask, 0.2 ml/kg of an anesthetic combination (ketamine, 150 mg/1.5 ml; xylazine, 30 mg/1.5 ml; and distilled water, 1 ml) was subcutaneously injected before surgery. During the operation, booster doses of 0.1 ml/kg were given as required. All animals were placed in the supine position and secured to the operating table. BCCAL was performed on the anterior cervical region. After making a mid-cervical medial incision 3 cm long, the common carotid artery-vagal nerve-jugular vein-sympathetic chain was located on each side. The common carotid arteries were dissected and BCCAL was performed on 13 animals in the experimental group but not on the sham animals. The animals in the sham group also underwent carotid sheath opening through longitudinal neck dissection. The animals were allowed to recover and were sacrificed 1 month later. All STGs were removed bilaterally from each animal and placed in 10% formalin solution for 7 days. The STGs from both sides were dissected and embedded horizontally in paraffin blocks in a manner that permitted observation of all the roots during the histological examination. The physical dissector method was used to estimate the number of neurons in each STG [6].

To estimate neuron numbers of a STG, two consecutive sections (dissector pairs) obtained from reference tissue samples were mounted on each slide. The order of paired reference sections was also reversed in order to double the number of dissector pairs without the need to cut new sections. The mean density of normal neurons in the STG (Nv/Gv) per mm^3 was estimated using the formula $Nv/Gv = \Sigma Q^-/\Sigma Axd$, where Q^-N is the total number of counted neurons appearing only in the reference sections; d is the section thickness, and A is the area of the counting frame. ΣA was estimated for the set of dissectors by $\Sigma A = \Sigma Pa$, where ΣPa is the total number of counting frame set points and a is a constant area associated with the set points. The areas of the counting frames are shown in Fig. 2a, b, and the specimens were blindly evaluated by two examiners. a and b were consecutive sections taken 5 µm apart, in which a neuronal nucleus present in a was absent in b (Fig. 2a, b). The Cavalieri volume estimation method was used to obtain the total number of neurons in each specimen, which was calculated by multiplying the volume (mm^3) and neuron density in each STG. The number of normal and degenerated neurons in the STG was counted for each animal.

Statistical Analysis

Differences in heart rates and neuron density in stellate ganglia were analyzed with SPSS for Windows v.12.0 (SPSS Inc., Chicago, IL, USA), using the Kruskal–Wallis and Mann–Whitney *U* tests. Differences were considered significant at $p<0.05$.

Results

Two animals in the BCCAL group died within the first week following surgery, after experiencing ischemic attacks, loss of consciousness, convulsions, and breathing disturbances. The remaining animals ($n=11$) were followed for 1 month.

Figure 1 shows the digital subtraction angiography (DSA) appearances of the caroticovertebral system with common carotid (CCA), vertebral (VA), and subclavian arteries (SCA) at the base. Schematic representations of the caroticovertebrobasilar system and the cervical sympathetic chain (SSG—superior sympathetic ganglion, VA—vertebral artery, MSG—middle cervical ganglion, ISG—inferior cervical ganglion, SC—sympathetic cervical chain, STG—stellate ganglion) (a) and electrocardiographic monitoring of a normal rabbit (b) are also shown in Fig. 1. Figure 2a, b shows the stereologic cell counting of the STG in a rabbit. The physical dissector method was applied, in which micrographs in the same fields of view (a, b) were taken from two parallel, adjacent thin sections separated by a distance of 5 µm. The upper and right lines

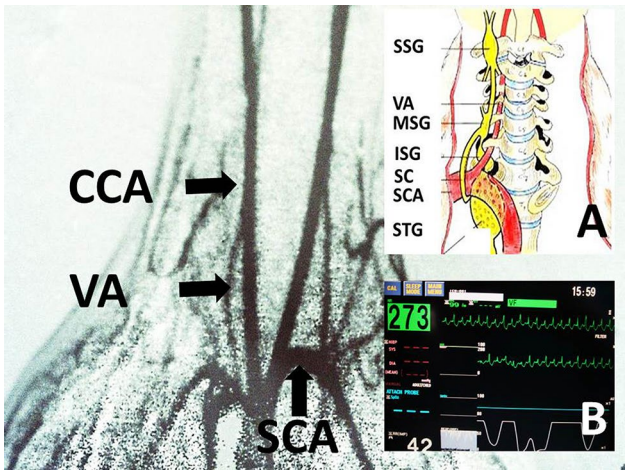

Fig. 1 Digital subtraction angiography (DSA) appearances of the caroticovertebral system with common carotid (CCA), vertebral (VA), and subclavian arteries (SCA) in the base (taken from Prof.Dr. Mehmet Dumlu Aydin's archive). A schematic representation of the caroticovertebrobasilar system and cervical sympathetic chain (*SSG* superior sympathetic ganglion, *VA* vertebral artery, *MSG* middle cervical ganglion, *ISG* inferior cervical ganglion, *SC* sympathetic cervical chain, *STG* stellate ganglion) (with permission of Assoc. Prof. Dr. Selim Kayaci) is shown in **a** and electrocardiographic monitoring of a normal rabbit is shown in **b**

in the unbiased counting frames represent the inclusion lines, and the lower and left lines, including the extensions, are exclusion lines. The neuronal nucleoli touching the inclusion lines were excluded, and the nucleolus profiles touching the inclusion lines and located inside the frame were counted as dissector particles unless their profiles extended up to the reference section. The number of neurons from the two dissectors occurs in a volume given by the product of the counting frame area and the distance between the sections. The numerical density of the neurons is calculated as $NvGN = \Sigma Q–GN/txA$. In this application, the nucleoli marked with '1, 2, 4, 5, 6' are dissector particles in a. Section b shows them as they disappeared. The nucleoli marked with '3, 7, 8, 9' are not dissector particles in a. Section b shows '3, 7, 8, 9' as they disappeared (LM, H&E, ×10). Figure 3 shows the DSA appearances of the caroticovertebral system after common carotid artery ligation (LCCA), vertebral (VA), subclavian artery (SCA) aorta (a), disappearance of the carotid system, electrocardiographic monitoring of a rabbit with a low heart rate (a), and degenerated STG neurons (LM, H&E, ×4, b). Figure 4 shows electrocardiographic monitoring of a rabbit with bradycardia (a); degenerated neurons of STG (LM, H&E, ×4/Base/black arrow) and apoptotic neurons (LM, TUNEL, ×10, b).

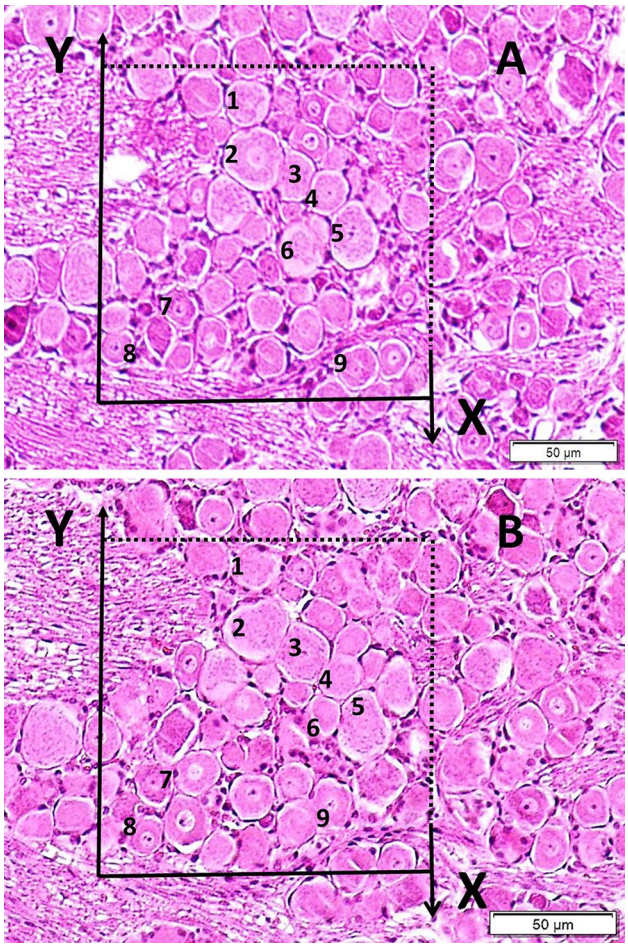

Fig. 2 **a, b** Stereological cell counting of the stellate ganglion (STG) in a rabbit. The physical dissector method was applied, in which micrographs in the same fields of view (**a, b**) were taken from two parallel, adjacent thin sections separated by a distance of 5 µm. The upper and right lines in the unbiased counting frames represent the inclusion lines, and the lower and left lines, including the extensions, are exclusion lines. The neuronal nucleoli touching the inclusion lines were excluded, and the nucleolus profiles touching the inclusion lines and located inside the frame were counted as dissector particles unless their profile extended up to the reference section. The number of neurons from the two dissectors occurs in a volume given by the product of the counting frame area and the distance between the sections. The numerical density of the neurons is calculated as $NvGN = \Sigma Q^{-}GN/txA$. In this application, the nucleoli marked with '1, 2, 4, 5, 6' are dissector particles in **a**. Section **b** shows them as they disappeared. The nucleoli marked with '3, 7, 8, 9' are not dissector particles in **a**. Section **b** shows '3, 7, 8, 9' as they disappeared (LM, H&E, ×10)

Numerical Values of the Study

The heart rates of all normal and control animals were determined as 294 ± 21/min, the mean normal neuron density in the STG was $10.340 \pm 954/mm^3$, and the degenerated neuron density was $12 \pm 3/mm^3$ in the GI group ($p > 0.5$). The heart rates and degenerated neuron densities

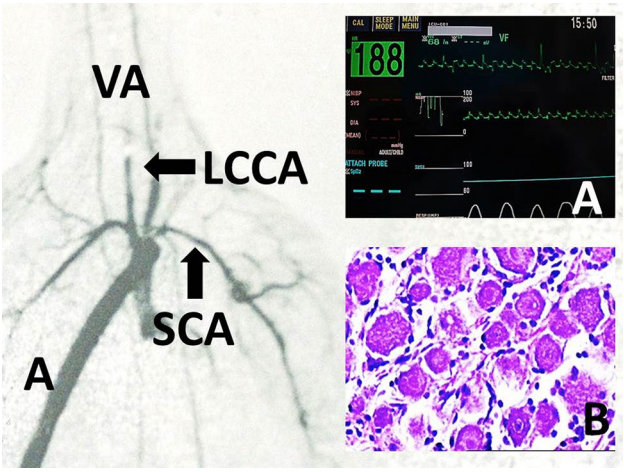

Fig. 3 Digital subtraction angiography (DSA) appearances of the caroticovertebral system after common carotid artery ligation (LCCA), vertebral (VA), subclavian artery (SCA) and aorta (A), and disappearance of carotid system are seen in the figure base (taken from Prof. Dr. Mehmet Dumlu Aydin's archive). Electrocardiographic monitoring of a rabbit with low heart rate (**a**) and degenerated STG neurons (LM, H&E, ×4, **b**) are shown

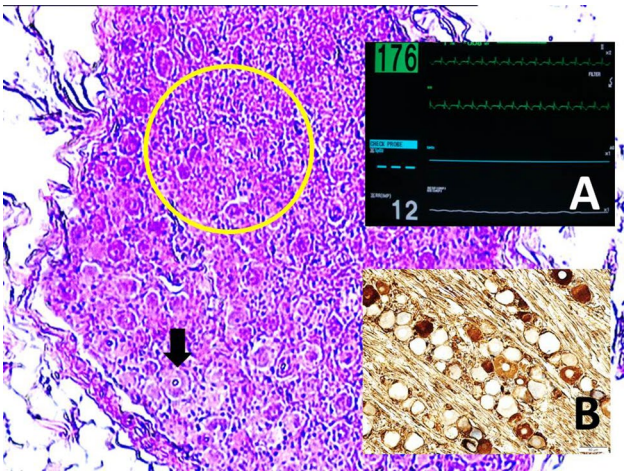

Fig. 4 Electrocardiographic monitoring of a rabbit with bradycardia (**a**); degenerated neurons of STG (LM, H&E, ×4/Base/black arrow) and apoptotic neurons (LM, TUNEL, ×10, **b**)

of STGs were recorded as 267 ± 19/min and 237 ± 45/mm^3 for GII ($p < 0.005$ for GII vs. GI); and 190 ± 11/min, 1421 ± 230/mm^3 for GIII ($p < 0.0001$ for GIII vs. GI and $p < 0.005$ for GIII vs. GII). An inverse and meaningful association was observed between the heart rate and the degenerated neuronal density in the STG. A low degenerated neuron density in the STG may protect against bradycardia following BCCAL.

Discussion

The BCCAL procedure produces a major redistribution of blood to the head, with increased and retrograde blood flow through the vertebral and basilar arteries. Important morphologic and histopathologic changes occur in the vertebral, basilar, posterior communicating, and posterior cerebral arteries and in the neck vessels within 4 months [1]. We previously provided elaborate observations of the significant collateral circulation, neovascularisation, and cerebral aneurysm formation occurring 2–4 months after BCCAL [7–9].

Carotid stenosis causes reduced distensibility of the carotid wall and impaired heart rate variability. Because the carotid bodies supplying the arteries arise directly from the carotid sinus, and because severe damage of the carotid baroreceptors and chemoreceptors (carotid bodies) and narrowing of the supplying arteries are features of carotid stenosis [10, 11], these changes have mainly been attributed to dysfunction of the carotid bodies [12, 13]. A cadaveric study indicated that the primary arterial supply to the sympathetic chain and ganglia was, superior to inferior, the ascending pharyngeal, ascending cervical, thyrocervical trunk, and supreme intercostal arteries [14].

The neuronal densities of the peripheral nerve ganglia are essential for the optimal nerve function on target organs, as many kinds of neurotransmitters, neuromodulators, and neurochemicals are produced by these ganglia [15]. The increased neuron density of the STG may result in overactivation of the cardiorespiratory organs by the sympathetic system [2, 8]. For example, Aydin et al. reported that the lower neuron density of the petrosal ganglion may be responsible for higher blood pressure [16]. Anatomic studies have demonstrated that aging increases the fibrous and fatty tissue in the AV node and His bundle [17, 18]. Another anatomic study has described a decrease in the autonomic innervation of the AV conduction system with aging, thereby potentially reducing the usual and expected effects of autonomic input to the heart [19].

A previous report indicated that persistent bradycardia resolved within a few hours of post carotid artery stenting (CAS) in a patient with concomitant carotid and coronary artery diseases. In that case, despite correction of the coronary lesions and a normal electrophysiology profile (normal AH, HV, RR, PR, QRS, QT intervals, sinus node recovery time, and corrected sinus node recovery time), the persistent bradycardia did not resolve; however, the patient had severe bilateral carotid artery stenosis. Those authors concluded that persistent bradycardia was a result of this significant internal carotid artery disease and the correction of bradycardia within a few hours post-CAS was a remarkable phenomenon that needs further investigation [20].

The literature contains conflicting results regarding the heart rate response to bilateral carotid occlusion (BCO), depending on the species studied. Tachycardia or no change in heart rate was found in dogs [21, 22]. A rise in heart rate during BCO was also observed in rabbits [23], while fetal sheep exhibited bradycardia [24]. Despite these heterogeneous results, some evidence indicates that the right STG fibers are responsible for heart rate control, while the left STG fibers supply the coronary vessels and myocardium [25–29]. A previous study [13] indicated an association between impaired baroreflex sensitivity and bilateral, but not unilateral, carotid atherosclerosis. Interestingly, no correlation was found between a baroreflex sensitivity reduction and the severity of carotid atherosclerosis.

The neuron density of the CST may play an important role in the regulation of the heart rate and in the continuation of the cerebral/coronary circulation in normal ranges. A low neuron density in the STG should be considered a dangerous risk factor for the pathogenesis of severe bradycardia development in stenoocclusive carotid artery disease. Although a low neuron density of the STG may have a beneficial effect in acutely developed stenoocclusive carotid artery disease, it may be dangerous due to the decreased sympathetic effects because of the higher cardiac energy requirements of chronic stenoocclusive carotid disease. The determined electrical alternation, characterized by low–high voltage and QRS complex time variabilities, may indicate that these electrocardiographic abnormalities originate from the ischemic degenerative changes of the STG. In other words, the heart rhythm variabilities may originate from sympathovagal imbalances between the ischemic STG and indirectly activated vagal nerves.

The cervical sympathetic chain on each side consists of a superior cervical, a middle cervical, and a stellate ganglion, followed by a ganglion located at the level of each rib [30]. We suggest that reduced activity in any of these ganglia, by means of degenerated STG neurons, results in denervation injury, which may affect all these ganglia because of their serial connection. Furthermore, reduced CST nerve activity in stenoocclusive carotid disease may lead to decreased heart rates due to the direct connection between the CST and the vagal nerves.

Conclusions

In the present study, we found a higher mean heart rate in animals with high neuron density than with lower neuron density. These data suggest that atherosclerotic disease at the carotid bifurcation can lead to CST ischemia, with a consequent upregulation of parasympathetic activity. Baroreceptors and chemoreceptors situated at the carotid bifurcation can also behave maladaptively in the setting of stenoocclusive carotid artery disease. We propose that elderly patients presenting with bradyarrhythmias and neurologic symptoms should undergo a carotid duplex ultrasonography before deciding on a permanent pacemaker.

Study Limitations

Limitations of this study include the fact that the heart rate responses were evaluated in anesthetized animals and in the short term after occlusion of the bilateral carotid system. As such, the data may not translate completely to predict the function of the human CST. Studies were also undertaken in normal animals, so any potential cardiac disease-induced changes in central–peripheral interactions for cardiac control were not evaluated.

Compliance with Ethical Standards

Conflict of interest All authors declare that they have no conflict of interest.

References

1. Oldendorf, W. H. (1989). Trophic changes in the arteries at the base of the rat brain in response to bilateral common carotid ligation. *Journal of Neuropathology & Experimental Neurology, 48*, 534–547.
2. Onen, M. R., Yilmaz, I., Ramazanoglu, L., Tanrıverdi, O., Aydin, M. D., Kanat, A., et al. (2016). Rational roots of sympathetic overactivity by neurogenic pulmonary edema modeling arising from sympathyco-vagal imbalance in subarachnoid hemorrhage: An experimental study. *World Neurosurgery, 92*, 463–470.
3. Yilmaz, I., Eseoglu, M., Onen, M. R., Tanrıverdi, O., Kilic, M., Yilmaz, A., et al. (2017). Inverse association between basilar artery volume and neuron density in the stellate ganglion following bilateral common carotid artery ligation: An experimental study. *World Neurosurgery, 100*, 138–143.
4. Huang, B., Yu, L., Scherlag, B. J., Wang, S., He, B., Yang, K., et al. (2014). Left renal nerves stimulation facilitates ischemia-induced ventricular arrhythmia by increasing nerve activity of left stellate ganglion. *Journal of Cardiovascular Electrophysiology, 25*, 1249–1256.
5. Lujan, H. L., Palani, G., Zhang, L., & DiCarlo, S. E. (2010). Targeted ablation of cardiac sympathetic neurons reduces the susceptibility to ischemia-inducedsustained ventricular tachycardia in conscious rats. *American Journal of Physiology-Heart and Circulatory Physiology, 298*, H1330–H1339.
6. Sterio, D. C. (1984). The unbiased estimation of number and sizes of arbitrary particles using the disector. *Journal of Microscopy, 134*, 127–136.
7. Aydin, M. D., Ozkan, U., Gündoğdu, C., & Onder, A. (2002). Protective effect of posterior cerebral circulation on carotid body ischemia. *Acta Neurochirurgica, 144*, 369–372.
8. Eseoglu, M., Yilmaz, I., Karalar, M., Aydin, M. D., Kayaci, S., Gundogdu, C., et al. (2014). The role of sympathectomy on the regulation of basilar artery volume changes in stenoocclusive carotid artery modeling after bilateral common carotid artery ligation: An animal model. *Acta Neurochirurgica (Wien), 156*, 963–969.

9. Aygul, R., Aydin, M. D., Kotan, D., Demir, R., Ulvi, H., Karalar, M., et al. (2013). Role of the trigeminal system on posterior communicating artery remodelization after bilateral common carotid artery ligation. *Analytical and Quantitative Cytopathology and Histopathology 35*, 217–225.
10. Jago, R., Heath, D., & Smith, P. (1982). Structure of the glomic arteries. *The Journal of Pathology, 138*, 205–218.
11. Milei, J., Lavezzi, A. M., Bruni, B., Grana, D. R., Azzato, F., & Matturri, L. (2009). Carotid barochemoreceptor pathological findings regarding carotid plaque status and aging. *Canadian Journal of Cardiology, 25*, e6–e12.
12. Chao, A. C., Chern, C. M., Kuo, T. B., Chou, C. H., Chuang, Y. M., Wong, W. J., et al. (2003). Noninvasive assessment of spontaneous baroreflex sensitivity and heart rate variability in patients with carotid stenosis. *Cerebrovascular Diseases, 16*, 151–157.
13. Nasr, N., Pavy-Le Traon, A., & Larrue, V. (2005). Baroreflex sensitivity is impaired in bilateral carotid atherosclerosis. *Stroke, 36*, 1891–1895.
14. Tubbs, R. S., Salter, G., Wellons, J. C. 3rd, & Oakes, W. J. (2002). Blood supply of the human cervical sympathetic chain and ganglia. *European Journal of Morphology, 40*, 283–288.
15. Moskowitz, M. A., Renhard, J. F., Romero, J., Melamed, E., & Pettibone, D. J. (1979). Neurotransmitters and the fifth cranial nerve: Is there a relation to the headache phase of migraine? *Lancet, 2*, 883–885.
16. Aydin, M. D., Bayram, E., Atalay, C., Aydin, N., Erdogan, A. R., Gundogdu, C., et al. (2006). The role of neuron numbers of the petrozal ganglion in the determination of blood pressure. An experimental study. *Minimally Invasive Neurosurgery, 49*, 328–330.
17. Bharati, S., & Lev, M. (1992). The pathologic changes in the conduction system beyond the age of ninety. *American Heart Journal, 124*, 486–496.
18. Song, Y., Laaksonen, H., Saukko, P., Toivonen, S., & Zhu, J. (2001). Histopathological findings of cardiac conduction system of 150 finns. *Forensic Science International, 119*, 310–317.
19. Chow, L. T., Chow, S. S., Anderson, R. H., & Gosling, J. A. (2001). Autonomic innervation of the human cardiac conduction system: changes from infancy to senility-an immunohistochemical and histochemical analysis. *The Anatomical Record, 264*, 169–182.
20. Polydorou, A., Megalooikonomos, P., Portinos, A., Prapa, E., Kara, P., Tsiga, A., et al. (2010). Persistent bradycardia in a patient with coronary artery disease and concomitant carotid artery disease. *Hospital Chronicles, 5*(1 Sup), 101–104.
21. Kirby, D. A., & Vatner, F. (1987). Enhanced responsiveness to carotid baroreceptor unloading in conscious dogs during development of perinephritic hypertension. *Circulation Research, 61*, 678–686.
22. Vatner, S. F., & Manders W. T. (1979). Depressed responsiveness of the carotid sinüs reflex in conscious newborn animals. *American Journal of Physiology-Heart and Circulatory Physiology, 237*, H40–H43.
23. Kumagai, K., & Reid, I. A. (1994). Losartan inhibits sympathetic and cardiovascular responses to carotid occlusion. *Hypertension, 23*, 827–831.
24. Schröder, H. J., Rybakowski, C., Eisermann, K., Tchirikov, M., & Ostermann, S. (2000). Unloading of baroreceptors by carotid occlusion does not increase heart rate in fetal sheep. *European Journal of Obstetrics & Gynecology and Reproductive Biology, 92*, 265–272.
25. Fujiki, A., Masuda, A., & Inoue, H. (1999). Effects of unilateral stellate ganglion block on the spectral characteristics of heart rate variability. *Japanese Circulation Journal, 63*, 854–858.
26. Rogers, M. C., Abildskov, J. A., & Preston, J. B. (1973). Cardiac effects of stimulation and block of the stellate ganglion. *Anesthesiology, 39*, 525–533.
27. Schwartz, P. J. (1984). The rationale and the role of left stellectomy for the prevention of malignant arrhythmias. *Annals of the New York Academy of Sciences, 427*, 199–221.
28. Song, J. G., Hwang, G. S., Lee, E. H., Leem, J. G., Lee, C., Park, P. H., et al. (2009). Effects of bilateral stellate ganglion block on autonomic cardiovascular regulation. *Circulation Journal, 73*, 1909–1913.
29. Vaseghi, M., Zhou, W., Shi, J., Ajijola, O. A., Hadaya, J., Shivkumar, K., et al. (2012). Sympathetic innervation of the anterior left ventricularwall by the right and left stellate ganglia. *Heart Rhythm, 9*, 1303–1309.
30. Kawashima, T. (2011). Anatomy of the cardiac nervous system with clinical and comparative morphological implications. *Anatomical Science International, 86*, 30–49.